8120 *Biochemistry* **2009,** *48,* 8120–8128
DOI: 10.1021/bi900923b

BIOCHEMISTRY
including biophysical chemistry & molecular biology
Article

Prion Proteins with Pathogenic and Protective Mutations Show Similar Structure and Dynamics[†]

Sung-Hun Bae,[‡] Giuseppe Legname,[§,||] Ana Serban,[§] Stanley B. Prusiner,[§] Peter E. Wright,[‡] and H. Jane Dyson*[,‡]

[‡]*Department of Molecular Biology and Skaggs Institute for Chemical Biology, The Scripps Research Institute, La Jolla, California 90237, and* [§]*Institute for Neurodegenerative Diseases and Department of Neurology, University of California, San Francisco, California 94143*
[||]*Present address: Neurobiology Sector, Scuola Internazionale Superiore di Studi Avanzati (SISSA), Trieste, Italy*

Received June 2, 2009; Revised Manuscript Received July 16, 2009

ABSTRACT: Conformational change in the prion protein (PrP) is thought to be responsible for a group of rare but fatal neurodegenerative diseases of humans and other animals, including Creutzfeldt−Jakob disease and bovine spongiform encephalopathy. However, little is known about the mechanism by which normal cellular PrPs initiate and propagate the conformational change. Here, we studied backbone dynamics of the inherited pathogenic mutants (P101L and H186R), protective mutants (Q167R and Q218K), and wild-type mouse PrP(89−230) at pH 5.5 and 3.5. Mutations result in minor chemical shift changes around the mutation sites except that H186R induces large chemical shift changes at distal regions. At lower pH values, the C-terminal half of the second helix is significantly disordered for the wild-type and all mutant proteins, while other parts of the protein are essentially unaffected. This destabilization is accompanied by protonation of the partially exposed histidine H186 in the second helix of the wild-type protein. This region in the mutant protein H186R is disordered even at pH 5.5. The wild-type and mutant proteins have similar microsecond conformational exchange near the two β-strands and have similar nanosecond internal motions in several regions including the C-terminal half of the second helix, but only wild type and P101L have extensive nanosecond internal motions throughout the helices. These motions mostly disappear at lower pH. Our findings raise the possibility that the pathogenic or dominant negative mutations exert their effects on some non-native intermediate form such as PrP* after conversion of cellular PrP (PrP^C) into the pathogenic isoform PrP^{Sc} has been initiated; additionally, formation of PrP^{Sc} might begin within the C-terminal folded region rather than in the disordered N-terminal region.

Prion diseases are a group of rare but fatal neurodegenerative disorders that pathologically manifest accumulation of protease-resistant aggregates of prion protein (PrP)[1] in affected brain regions (*1*−*4*). These disorders appear as sporadic, dominantly heritable, and transmissible maladies that include Creutzfeldt−Jakob disease (CJD), Gerstmann−Sträussler−Scheinker syndrome (GSS), fatal familial insomnia (FFI), and kuru in humans, bovine spongiform encephalopathy in cattle, scrapie in sheep, and chronic wasting disease in elk and deer.

PrP is a highly conserved glycoprotein that contains two glycosylation sites and is linked to the external surface of the cell through a glycosylphosphatidylinositol (GPI) anchor. NMR studies revealed that the recombinant PrP consists of a largely unfolded N-terminal region and a folded C-terminal domain encompassing three α-helices (α1, α2, and α3) and two short β-strands (β1 and β2), with a single disulfide bond bridging α2 and α3 (*5*, *6*).

All prion diseases are thought to be caused by a profound conformational change, which occurs when the normal, cellular isoform (PrP^C) is converted to the pathological form (PrP^{Sc}) in the absence of any detectable covalent modification. PrP^C is rich in α-helical structure; in contrast, PrP^{Sc} forms aggregates and is β-sheet rich (*7*, *8*). Many but not all forms of PrP^{Sc} are resistant to proteolysis (*9*). The molecular mechanism by which PrP^{Sc} initiates and propagates a conformational change during prion propagation remains unclear. In particular, the conditions necessary *in vivo* for the formation of PrP^{Sc} such as pH, redox environment, posttranslational modifications, and cofactor(s) remain elusive. There is ongoing controversy regarding whether the structure of PrP^{Sc} is amyloid or an intermediate β-sheet-rich oligomer on the pathway to amyloid formation. *In vitro* conversion of PrP^C into amyloid does not, in general, lead to the formation of PrP^{Sc}; most of the converted molecules appear to be in a noninfectious amyloid conformation whose structure is quite different from that of PrP^{Sc} (G. Stubbs, personal communication).

Exposure of scrapie-infected neuroblastoma (ScN2a) cells to weak bases inhibited the formation of nascent PrP^{Sc}. Acidic endosomes seem to play an important role in intracellular trafficking of PrP^{Sc} from cholestrerol-rich microdomains on the cell surface to lysosomes (*10*−*13*). Additionally, the

[†]This work was supported by Grant AG21601 from the National Institutes of Health. S.-H.B. was supported by a fellowship from the Korea Research Foundation Grant funded by the Korean Government (MOEHRD, Basic Research Promotion Fund) (KRF-2006-352-C00036).

*Corresponding author. Tel: 858-784-2223. Fax: 858-784-9822. E-mail: dyson@scripps.edu.

[1]Abbreviations: PrP, prion protein; GSS, Gerstmann−Sträussler−Scheinker syndrome; CJD, Creutzfeldt−Jakob disease; FFI, fatal familial insomnia; NMR, nuclear magnetic resonance; R_1, longitudinal relaxation rate; R_2, transverse relaxation rate; NOE, nuclear Overhauser effect; CPMG, Carr−Purcell−Meiboom−Gill; S^2, order parameter.

 Published on Web 07/20/2009

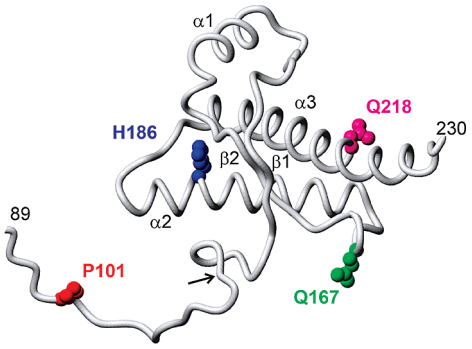

FIGURE 1: Location of the sites of the mutations on the 3D structure of mouse PrP (PDB ID: 1xyx) (*26*). In order to illustrate the position of P101, the unstructured N-terminal tail is modeled as a random-coil segment from the N-terminus at residue 89 to the position of the arrow, where the published coordinates begin.

conversion of PrP *in vitro* into the protease-resistant form accelerates at acidic pH in the presence of denaturant (*14*), and a β-sheet-rich unfolding intermediate of PrP is exclusively observed at low pH (*15*).

In order to explore the factors that may affect the rate or propensity for the conversion of PrP^{C} into PrP^{Sc}, we compared the solution behavior of four mutant PrPs in terms of deformation and altered flexibility which should modulate the initiation of spontaneous conversion and/or the interaction with intermediates on the route of conversion (*16*, *17*). The positions of these mutation sites are shown mapped on the structure of the mouse prion protein (*5*) with a modeled N-terminal tail in Figure 1. The human equivalents of the mouse P101L and H186R mutations cause familial prion diseases (*18*, *19*). By contrast, the Q167R and Q218K mutations manifest a dominant negative phenotype in sheep and humans, respectively (*20*−*22*). Since the conversion of PrP^{C} into PrP^{Sc} requires an acidic endosomal compartment (*13*), we compared the structural and dynamic changes induced by acidic pH on the wild-type and four mutant mouse PrPs (residues 89−230) by measuring and analyzing backbone ^{15}N NMR relaxation. We found that the wild-type and mutant PrPs exhibited many similarities and relatively few differences in their dynamic features.

Our findings raise the possibility that the conformational change, which features in the conversion of PrP^{C} into PrP^{Sc}, begins in the C-terminal folded region. Our data also suggest that some PrP mutations do not alter the initial steps in the conformational transition that PrP undergoes.

MATERIALS AND METHODS

Sample Preparation. $^{15}N/^{13}C$-labeled and/or ^{15}N-labeled recombinant mouse PrP(89−230) of wild type, P101L, Q167R, H186R, and Q218K were expressed in *Escherichia coli*, purified, and refolded as previously described (*6*, *23*). NMR samples were prepared in 20 mM sodium acetate, pH 5.5 or 3.5, 90% H_2O/10% D_2O, and 0.05% sodium azide. The protein concentration was 0.1−0.6 mM (Supporting Information Table S1).

NMR Resonance Assignments and Relaxation Measurements. Backbone resonances Cα, Cβ, C′, N, and H of wild-type mouse PrP(89−230) were assigned by using three-dimensional (3D) HNCACB, CBCA(CO)NH, HNCO, ^{15}N-edited NOESY-HSQC (τ_m = 150 ms), ^{15}N-edited TOCSY-HSQC (τ_m = 80 ms), (*24*) and the deposited chemical shift data of Syrian hamster PrP(90−231) (BMRB ID: 4307) (*25*). Backbone assignments were transferred from the wild-type to the four mutant PrPs and confirmed using ^{15}N-edited NOESY-HSQC (τ_m = 150 ms) and ^{15}N-edited TOCSY-HSQC (τ_m = 80 ms). No backbone resonances were observed for residues 168−174 in wild-type and all four mutant PrPs as reported previously for wild type (*5*, *26*). Backbone resonances for residues 187−188 of the H186R mutant protein were not observed due to line broadening (Supporting Information Figure S1). The histidine imidazole resonances $^{1}H\delta2$, $^{1}H\varepsilon1$, $^{15}N\delta1$, and $^{15}N\varepsilon2$ of wild-type mouse PrP(89−230) were assigned by two-dimensional (2D) (Hβ)Cβ(Cγ-Cδ)Hδ (*27*) and by 2D long-range $^{1}H-^{15}N$ heteronuclear multiple-quantum coherence (HMQC) experiments (*28*). Protonation states of the histidines were examined using a 2D long-range HMQC in which the ^{15}N carrier frequency and sweep width were set to 180 and 30 ppm, respectively, and the delay during which ^{15}N and ^{1}H signals become antiphase was set to 4.5 ms (*29*). ^{15}N T_1, T_2, and $[^{1}H]-^{15}N$ NOE were measured on Bruker 500 and 600 MHz spectrometers at 298 K using pulse sequences described previously (*30*, *31*). Ten spectra were acquired using relaxation delays of 0.011*, 0.161, 0.33*, 0.495, 0.66*, 0.825, and 1.1 s for T_1 and 6*, 18, 34, 50*, 66, 90, and 114* ms for T_2 (the asterisks denote duplicate measurements). The $[^{1}H]-^{15}N$ NOE was measured from at least two sets of saturated and unsaturated spectra in which protons were saturated for 3.0 s or not after repetition delay. Repetition delay was 3.5, 3.5, and 3.0 s for T_1, T_2, and $[^{1}H]-^{15}N$ NOE experiments, respectively. All spectra were processed using nmrPipe (*32*). For obtaining relaxation rates R_1 ($=1/T_1$) and R_2 ($=1/T_2$), peak intensity was fitted to a single exponential decay function, $I(t) = I_0 \exp(-tR)$ in which t is the variable relaxation delay and R is the relaxation rate. The $[^{1}H]-^{15}N$ NOE was derived from the ratio of peak intensity measured in the saturated and unsaturated spectra ($=I_{sat}/I_{unsat}$). Experimental errors were estimated from standard deviations of the peak intensities of duplicate experiments. Carr−Purcell−Meiboom−Gill (CPMG) ^{15}N R_2 relaxation dispersion was measured at 298 K on Bruker 500 and 800 MHz spectrometers with total CPMG duration of 40 ms and recycling delay of 3 s (*24*). The ^{15}N longitudinal 2-spin-order exchange rates (zz-exchange) for H186R were measured and analyzed as described previously (*33*). Transverse cross-correlation (η_{xy}) between $^{15}N-^{1}H$ dipolar interactions and ^{15}N chemical shift anisotropy (CSA) was measured at 500 MHz and 298 K with dephasing delays ($\Delta\eta$) of 10, 25, and 40* ms (the asterisks denote duplicate measurements) (*34*).

Model-Free Analysis and Reduced Spectral Density Mapping. ^{15}N R_1, ^{15}N R_2, and $[^{1}H]-^{15}N$ NOE data sets acquired at 500 and 600 MHz were analyzed by an in-house computer program eMF (S.-H. Bae, unpublished), using the extended Lipari−Szabo formalism (*35*−*37*). An axially symmetric rotational diffusion tensor was optimized against the mouse PrP structure (PDB ID: 1xyx) (*26*) using selected residues with $[^{1}H]-^{15}N$ NOE > 0.65 which belong to α-helices and β-strands (Supporting Information Table S1). A best model for each residue was selected by the Bayesian information criterion (*38*−*40*) after excluding unrealistic model(s) that have $S^2 > 1$ or $\tau_e < 0$ ns or $R_{ex} < 0$ (*39*, *40*). Minimum errors were set to 3%, 3%, and 0.03 for ^{15}N R_1, ^{15}N R_2, and $[^{1}H]-^{15}N$ NOE, respectively. ^{15}N CSA and amide NH bond length were assumed to be −160 ppm and 1.02 Å. Reduced spectral densities $J(0)$, $J(\omega_N)$, and $J(0.89\omega_H)$ were mapped assuming that $J(\omega)$ is proportional to $1/\omega^2$ at high frequency around ω_H (*41*).

^{15}N R_2 Relaxation Dispersion Analysis. The ^{15}N R_2 relaxation dispersion data were fitted with the in-house computer

program GLOVE (J. C. Lansing, unpublished) using the general equation for two-site exchange that encompasses all conformational exchange time scales (*42*):

$$R_2(1/\tau_{cp}) = R_{20} + \frac{1}{2}\left[k_{ex} - \frac{1}{\tau_{cp}}\cosh^{-1}[D_+\cosh(\eta_+) - D_-\cos(\eta_-)]\right]$$

$$D_\pm = \frac{1}{2}\left[\pm 1 + \frac{\psi + 2\Delta\omega^2}{(\psi^2+\zeta^2)^{1/2}}\right]^{1/2}$$

$$\eta_\pm = \frac{\tau_{cp}}{\sqrt{2}}\left[\pm\psi + (\psi^2+\zeta^2)^{1/2}\right]^{1/2}$$

where $\psi = k_{ex}{}^2 - \Delta\omega^2$, $\zeta = -2\Delta\omega k_{ex}(p_A - p_B)$, τ_{cp} is the delay between 180° pulses in the CPMG pulse train, the p_a and p_b are populations of the two states A and B, k_{ex} is the exchange rate constant ($k_{ex} = k_{A\rightarrow B} + k_{B\rightarrow A}$), and $\Delta\omega$ is the ^{15}N chemical shift difference between two states.

Translational Diffusion Coefficient. Translational diffusion coefficients were measured at 298 K using the PFG-SLED (pulsed field gradient stimulated echo longitudinal encode−decode) NMR method (*43*). The PFG duration was 6.3 ms, and the self-diffusion delay was 80 ms. The PFG strength was varied from 5% to 90% in triplicate series of 1D spectra. The integral of peak intensity (I) is related to a relative diffusion coefficient, d, and relative gradient strength, G, by $I = I(0)\exp(-dG^2)$. The diffusion coefficient was calculated relative to the diffusion coefficient of lysozyme (1.08×10^{-6} cm^2 s^{-1}) (*43*).

RESULTS

Location and Nature of Mutations. The P101L and H186R mutations are associated with familial prion disease in humans; P101 and H186 are both highly conserved among mammalian species. These mutations occur in very different regions of the protein: P101 is located in the unstructured tail of the PrP 27−30 sequence (modeled in Figure 1), while H186 is packed into the core of the folded C-terminal domain, between α2, α3, and β2. It appears likely that the reasons why these mutations should favor conversion of PrP^C to other forms, including pathogenic forms, might differ. The dominant negative mutations Q167R and Q218K both occur in regions of the protein that are solvent-exposed, in the loop between β2 and α2 for Q167 and toward the end of the α3 helix for Q218. Neither of these residues is highly conserved among mammalian species: Q167 is replaced by Glu in the human sequence while Q218 is replaced by Glu in primate sequences.

Structural Changes of PrP Caused by Mutations and pH Change. The chemical shift perturbations caused at pH 5.5 by the P101L, Q167R, and Q218K mutations are small and are strictly localized to the mutation site and immediate neighbor residues (Figure 2A), consistent with the positions of these mutation sites in solvent-exposed areas of the protein that are low in secondary and tertiary structure (*5*, *6*). By contrast, the H186R mutation causes large chemical shift changes for the linker between α1 and β2 (Y156, Q159, Y162), α2 (Q185, T191, G194), and α3 (F197, E206) and minor chemical shift changes around β1. The relative magnitude of these changes is consistent with the position of residue 186 in the middle of α2 and the packing of the side chain into the core of the molecule. Nevertheless, even for H186R, the majority of the chemical shifts were

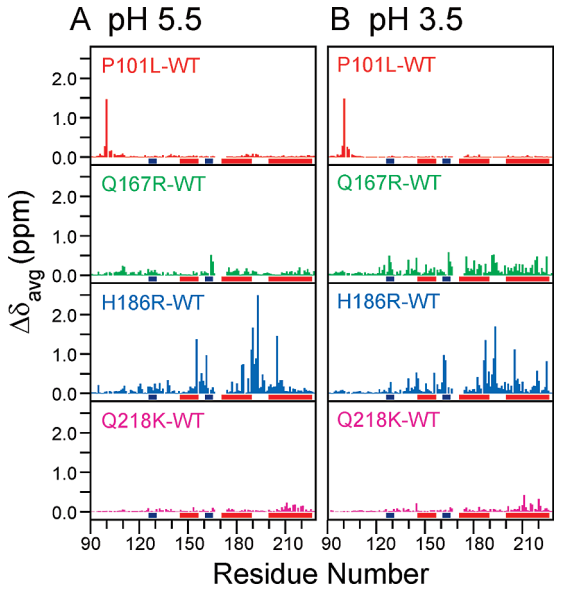

FIGURE 2: Perturbations caused by each mutation on the chemical shifts of ^{15}N and ^{1}H. Each panel shows the absolute value of an average chemical shift difference (Δδ) calculated by averaging amide ^{15}N and ^{1}H chemical shift differences using the empirical equation $\Delta\delta_{avg} = [\Delta\delta(^1H)^2 + \Delta\delta(^{15}N)^2]^{1/2}$, plotted as a function of primary sequence, and includes bars representing the positions of the α-helices (red) and β-strands (blue) in the 3D structure of the wild-type protein. (A) pH 5.5; (B) pH 3.5. Δδ data are not available for residues 168−174, for which no backbone resonances are observed (*5*, *26*).

virtually unaffected by the mutations, indicating that the overall structure of mouse PrP was not substantially altered in any of the mutations. Variations in the chemical shift upon changing conditions such as pH (3.5−5.5), KCl (0−150 mM), urea (0−1.5 M), and temperature (25−40 °C) showed that structural perturbations were most significant when the pH was changed (Supporting Information Figure S2). Chemical shift differences between mutant and wild-type proteins at pH 3.5 (Figure 2B) showed similar trends as those at pH 5.5. Since the chemical shift differences between mutants and wild type at pH 5.5 and 3.5 were similar, we inferred that all of the proteins were affected by acidic pH in similar ways.

Since acidic pH increases the probability of conversion to the pathogenic form (10−15), we anticipated that the inherited pathogenic PrP mutants might display different structural perturbations from the dominant negative PrP mutant or wild-type proteins upon acidification. However, the chemical shift differences between pH 5.5 and pH 3.5 were the same for wild type, P101L, Q167R, and Q218K, all of which showed similar and large chemical shift changes for residues from K184 to T198 (Figure 3). This region encompasses the C-terminal half of α2 and the connecting loop between helices α2 and α3. Among the affected residues, H186, T191, and K193 undergo the largest chemical shifts changes, suggesting that the C-terminal part of α2 plays a dominant role in the structural changes that occur at acidic pH. This region also has the largest chemical shift differences between pH 7.0 and pH 4.5 in human PrP(121−230) (*44*). In sharp contrast, the H186R mutant shows only small chemical shift differences for helix α2 (Figure 3), implying that this mutant does not undergo pH-dependent structural perturbations. These observations identify histidine 186 as responsible for the pH-dependent changes in the NMR spectra of the wild-type, P101L, Q167R, and Q218K mutant proteins. In addition, the wild type and all mutants share significant pH-dependent

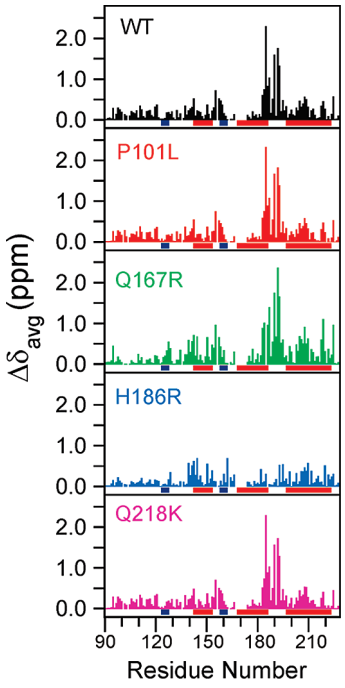

FIGURE 3: Perturbations caused by a change of pH from 5.5 to 3.5 for the wild-type and each of the mutant proteins. $\Delta\delta_{avg} = [\Delta\delta(^1H)^2 + \Delta\delta(^{15}N)^2]^{1/2}$.

chemical shift changes for residues 141−143 and 156−160 at the N- and C-termini of α2 and β2 and residues 205−214 in α3 (Figure 3), implicating a second titratable group.

A further decrease of pH to ≈2.1 resulted in severe line broadening of all resonances except for the N-terminal unfolded region (data not shown); this behavior was similar to that of the β-oligomer form of human PrP under moderately denaturating conditions (1 M urea, 0.2 M NaCl, 20 mM sodium acetate, pH 3.6) (*45*).

Backbone Dynamics of Wild-Type and Mutant PrPs. ^{15}N T_1, ^{15}N T_2, and $[^1H]-^{15}N$ NOE data sets were acquired at 298 K in 20 mM sodium acetate (pH 5.5 and 3.5) (Supporting Information Figure S3). Due to the presence of ≈35 unstructured residues at the N-terminus in PrP(89−230), which affects the tumbling of the folded domain, the rotational diffusion tensor could not be derived directly from the structure but was obtained from fitting the relaxation data sets to the wild-type mouse PrP(121−230) structure (PDB ID: 1xyx) (*26*) assuming that the overall structures of wild-type and mutant PrPs are not substantially different. Rotational correlation times calculated from the relaxation data were 9.8−11.9 ns, much larger than those expected from the empirical Stokes−Einstein estimation (≈8.4 ns) (*46*), and reflect the influence of the N-terminal unfolded region on the rotational tumbling of the C-terminal folded domain (*38*). The molecular tumbling of wild-type and mutant PrPs is slightly anisotropic ($D_\parallel/D_\perp \approx 1.4-1.7$) so that axially symmetric diffusion models fit the experimental data much better than an isotropic diffusion model (Supporting Information Table S1). In the fitting, the axis of the longest helix α3 coincides with the major principal axis of the rotational diffusion tensor. The dominant effect of α3 on the anisotropy of mouse PrP(89−230) is consistent with previous observations on the Syrian hamster proteins PrP(23−231 and 90−231) (*47*). Using fitted rotational diffusion tensors, the backbone dynamics of each residue were determined by model-free analysis (*35*−*37*). Previous attempts at model-free analysis of the Syrian hamster

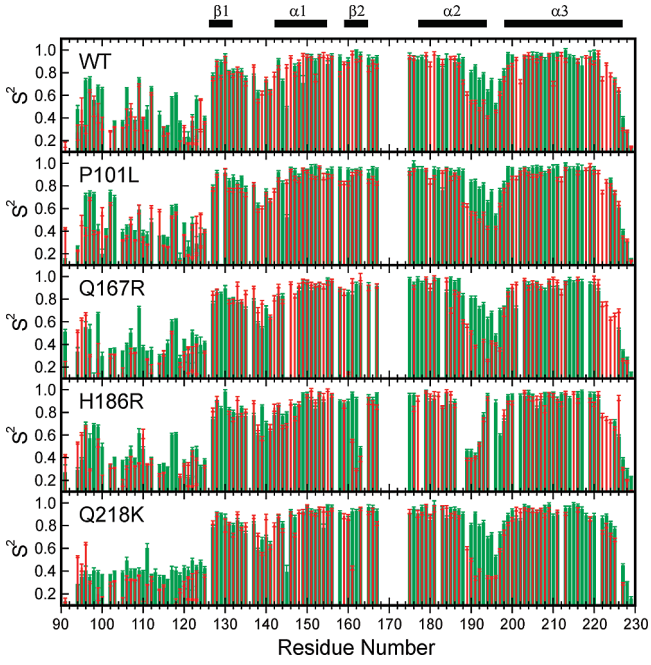

FIGURE 4: Order parameters (S^2) at pH 5.5 (green) and pH 3.5 (red) for wild-type and mutant proteins, calculated from model-free analysis of 500 and 600 MHz ^{15}N T_1, ^{15}N T_2, and $[^1H]-^{15}N$ NOE data sets measured at 298 K (data shown in Supporting Information Figure S3). For the N-terminal unfolded region (89−126), a local rotational diffusion model was used. For the folded region (127−230), a global axially symmetric rotational diffusion model was optimized using two-field relaxation data sets and the mouse PrP structure (PDB ID: 1xyx) (*26*). S^2 values are not available for residues 168−174 for which no backbone resonances are observed (*5*, *26*).

PrP(23−231 and 90−231) resulted in invalid order parameters ($S^2 > 1$) for many residues (*25*, *47*). The current analysis uses a nonisotropic rotational diffusion tensor (*48*) and a Bayesian information criterion (*39*, *40*) for model selection in conjunction with elimination of unrealistic models, which gives physically meaningful S^2 values for all of the fitted residues in wild type and mutants. Notably, a recent model-free analysis of a truncated form of the mouse PrP(113−231) using the isotropic rotational diffusion tensor has also resulted in valid S^2 values (*49*).

The motions of the N-terminal unfolded residues were analyzed with a local rotational diffusion model since their rotational tumbling should be independent of the C-terminal folded domain of the protein. The S^2 values in this region are ≈0.4, consistent with the highly flexible nature of the N-terminal terminal region (*6*). However, for all PrPs, there is a cluster of residues around H95 for which S^2 (≈0.6−0.8) ranges above the rest of the N-terminal unfolded region (Figure 4).

At pH 5.5 (green bars in Figure 4), the C-terminal folded region of all the proteins has an S^2 larger than 0.85, indicative of restricted backbone motion. However, two broad regions from β1 to α1 (residues ≈134−144) and from the C-terminal half of α2 to the beginning of α3 (residues ≈187−197) have lower S^2 values, indicative of backbone flexibility. All of the proteins, both wild type and mutants, share a similar S^2 pattern except that a short segment in the H186R mutant following residue 186 (≈187−193) shows a sharp decrease in S^2 while in the other proteins, the decrease was more gradual (Figure 4). At pH 3.5 (red bars in Figure 4), all proteins except H186R showed a substantial decrease in S^2 in the same region (residues 187−197) while the rest of the protein was essentially unaffected by a decrease of pH. S^2 for the H186R mutant was similar to the

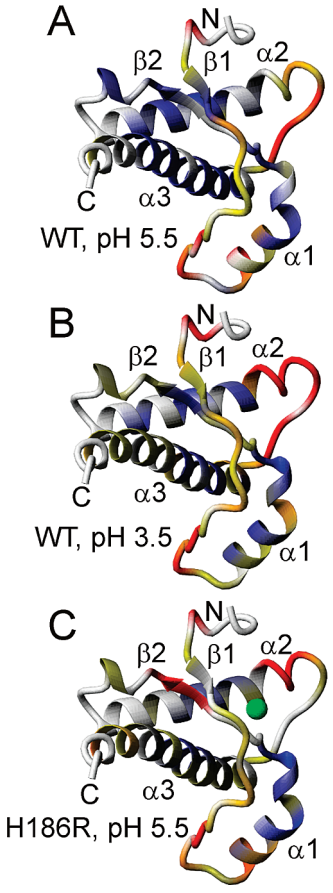

FIGURE 5: S^2 values are shown mapped on the mouse PrP structure (PDB ID: 1xyx) (*26*) as a continuous color scale: red for $S^2 < 0.6$, red to yellow for $0.6 \leq S^2 < 0.8$, and yellow to blue for $0.8 \leq S^2 < 1.0$. Prolines and residues for which S^2 is not determined due to spectral overlap, absence of data, or failure in fitting are shown in gray. (A) Wild-type PrP at pH 5.5. (B) Wild-type PrP at pH 3.5. (C) H186R mutant PrP at pH 5.5. The side chain of H186 is shown in green.

values observed for the N-terminal disordered tail. The variations in S^2 between pH 5.5 and pH 3.5 for the wild-type PrP are shown in Figure 5A,B and compared with those for the H186R mutant in Figure 5C. These observations suggest that residues 187−193 are disordered in the H186R mutant protein even at neutral pH.

Internal motions on the nanosecond time scale appear in both of the flexible segments (residues ≈134−144 and ≈187−197) (Figure 6). The nanosecond internal motions in the first segment propagate toward the N-terminus as far as A116. Reduced spectral densities $J(\omega_N)$ and $J(0.89\omega_H)$ could be used without the necessity for the assumptions made in the model-free analysis and provide further evidence for significant flexibility in these regions (Supporting Information Figure S4). The time scales of the internal motions are virtually unaffected by pH except for wild type and P101L. It is intriguing that only the wild-type and P101L proteins have extensive nanosecond internal motions throughout helices α1−α3 at pH 5.5 (Figure 6), even though high S^2 values indicate restricted backbone motion on the npicosecond to nanosecond time scale. Many of these nanosecond internal motions disappear at pH 3.5 (Figure 6). The combination of low amplitudes of picosecond to nanosecond backbone motion with extensive nanosecond internal motion in the same region has been reported in a number of cases (*50*). Partial aggregation of the wild-type and P101L mutant proteins could in principle be responsible for these apparently anomalous internal motions (*51*). However, on the basis of translational diffusion measurements, we could exclude this possibility: at the same concentration as the NMR relaxation measurements (0.55 mM), wild type, P101L, and Q218K have the same translational diffusion coefficients within experimental error (1.06 ± 0.01, 1.08 ± 0.01, and $1.08 \pm 0.02 \times 10^{-6}$ cm^2 s^{-1}, respectively, at 298 K).

All wild-type and mutant proteins show sharp increases in the R_2 relaxation rate near β1 and β2 at G130, V165, and D166 (Supporting Information Figure S3); such an increase is usually interpreted as evidence for conformational exchange on a microsecond to millisecond time scale. In order to separate the exchange contribution from R_2, exchange-free R_2 (R_{20}) was determined from transverse cross-correlation (η_{xy}) rates (*52*). Our findings show that these sites indeed undergo significant conformational exchange (Figure 7A). The Carr−Purcell−Meiboom−Gill (CPMG) ^{15}N R_2 relaxation dispersion data of G130, V165, and D166 show distinct differences between R_2 relaxation rates at 500 and 800 MHz even though each has small R_2 dispersion (< 5 s^{-1}) (Figure 7B). The exchange rate and the populations of the states were estimated from simultaneous fitting of the ^{15}N R_2 dispersion data of G130, V165, and D166 using the measured R_{20} and a two-site exchange model. These residues undergo fast exchange (7000 ± 2000 s^{-1}), where the population of the less favorable conformation is ≈0.4%. The fast conformational exchange of G130, V165, and D166 might be related to an intermediate time scale (microsecond to millisecond) conformational fluctuation in the loop connecting β2 and α2 (residues 168−174) which is most likely responsible for the severe line broadening of backbone resonances of these residues in wild-type and all four mutant PrPs (*5*, *26*). The loop between residues 170−175 has been implicated in disease (*53*, *54*); overexpression of PrP(170N, 174T) causes prion disease in the mouse (*55*). Interestingly, this loop region of human, cow, mouse, dog, and cat PrP is flexible, whereas that of elk, Syrian hamster, and bank vole is rigid (*6*, *26*, *54*, *56*−*58*), providing insights into species barriers for prion disease.

Unlike wild type and other mutants, the H186R mutant has two sets of resonances at residues Y162 and R163 in β2 at pH 5.5, with one set having chemical shifts similar to those of the other mutants and wild-type proteins (Supporting Information Figure S1). M128, L129, and G130 in β1 do not exhibit this slow conformational exchange although they have slightly broader resonances than other residues. We attribute these observations to a slow exchange between two conformations (the rate of exchange is too slow to be detected in the ^{15}N longitudinal 2-spin-order exchange (zz-exchange) experiments; data not shown). In the conformation with chemical shifts different from wild type and other mutants, Y162 shows significantly more flexibility ([^{1}H]−^{15}N NOEs are 0.19 ± 0.02 and 0.29 ± 0.04 at 500 and 600 MHz, respectively (Supporting Information Figure S3G) and S^2 is 0.34 ± 0.01) than the conformation with chemical shifts similar to wild type and the other mutants ([^{1}H]−^{15}N NOEs are 0.72 ± 0.09 and 0.61 ± 0.06 at 500 and 600 MHz, respectively, and S^2 is 0.92 ± 0.01). The H186R mutation appears to destabilize the β2 region, resulting in an equilibrium between ordered and disordered states. Interestingly, the Y162 peak originating from the more rigid conformation disappears at pH 3.5, while the other Y162 peak originating from the more flexible conformation remains ($S^2 = 0.30 \pm 0.01$), suggesting that the conformational equilibrium in the β2 region of H186R shifts toward the disordered state at lower pH.

Protonation of H186. Since our results indicated that H186 is involved in the destabilization of PrP that occurs as the pH is

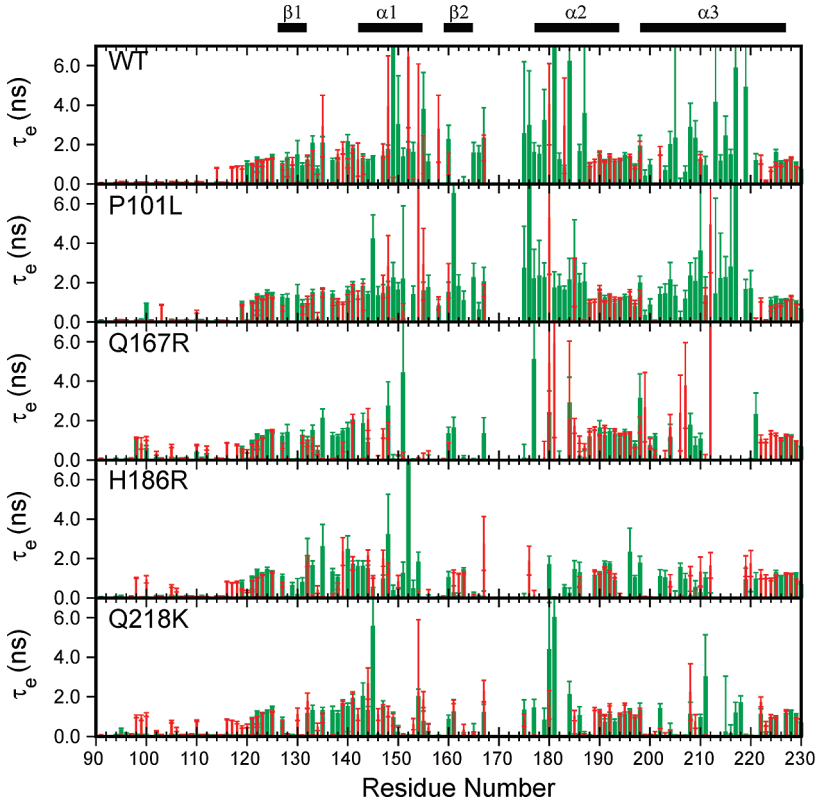

FIGURE 6: Correlation time of internal motion (τ_e) at pH 5.5 (green) and pH 3.5 (red). τ_e was calculated from model-free analysis of 500 and 600 MHz ^{15}N T_1, ^{15}N T_2, and [^{1}H]−^{15}N NOE data sets measured at 298 K. τ_e data are not available for residues 168−174 for which no backbone resonances are observed (*5*, *26*).

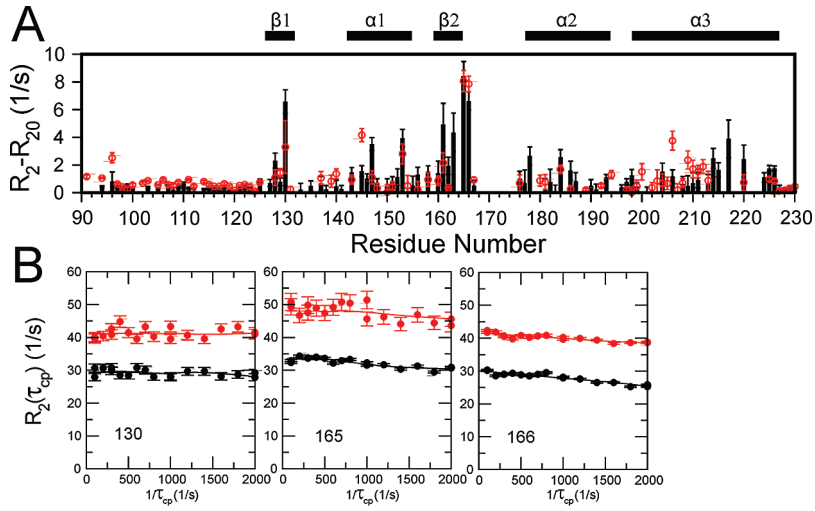

FIGURE 7: Conformational exchange. (A) Contribution of conformational exchange to R_2 relaxation. The transverse cross-correlation rate, η_{xy}, between the ^{15}N−^{1}H dipole−dipole interaction and the ^{15}N chemical shift anisotropy (CSA) was measured at 500 MHz for wild-type (black) and H186R (red) PrP(89−230) in pH 5.5 at 298 K. Exchange-free R_2 (R_{20}) was calculated by $R_{20} = -\eta_{xy}\sqrt{3}[(4c^2 + 3d^2)]/[12cdP_2(\cos\beta)]$ (*52*) in which $c = (\omega_N/\sqrt{3})\Delta\sigma$, $d = [\mu_0 h\gamma_N\gamma_H/8\pi^2](1/r^3_{NH})$, $P_2(x) = (3x^2 - 1)/2$ is the second-rank Legendre polynomial, h is Planck's constant, μ_0 is the permeability of free space, $\Delta\sigma$ is the ^{15}N CSA, r_{NH} is the amide NH bond length, and β is the angle between the principal axis of the ^{15}N CSA tensor and the amide NH bond vector. ^{15}N CSA, r_{NH}, and β were assumed to be −160 ppm, 1.02 Å, and 20°, respectively. (B) Carr−Purcell−Meiboom−Gill (CPMG) based ^{15}N R_2 relaxation dispersion of wild-type PrP(89−230) at pH 5.5 and 298 K. ^{15}N R_2 relaxation dispersion data of G130, V165, and D166 at 500 and 800 MHz were simultaneously fitted to the general equation for two-site exchange ($k_{ex} = k_{A\to B} + k_{B\to A}$, $p_A(=1 - p_B)$, p_B, $\Delta\omega$) (*42*) using the measured R_{20}. Data (filled circle) and fitted curves (solid line) at 500 MHz (black) and 800 MHz (red) are shown for G130, V165, and D166.

lowered, the protonation states of H186 were examined at pH 5.5 and 3.5 by ^{15}Nδ1 and ^{15}Nε2 chemical shifts (assignments for the side chain resonances of the five histidines are shown in Supporting Information Figure S5). The resonance frequencies of ^{15}Nδ1 and ^{15}Nε2 are at ≈168 and ≈250 ppm, respectively, in a neutral imidazole, and they both resonate at ≈177 ppm when completely protonated (*29*). Intermediate chemical shift values are indicative of fast exchange between protonated and deprotonated states. Among the five histidines in wild-type mouse PrP(89−230), H95, H110, H139, and H176 are exposed on the surface, and H186 is partially buried and surrounded by hydrophobic residues (*5*). The ^{15}Nδ1 and ^{15}Nε2 chemical shifts indicate that H110 and H176 are

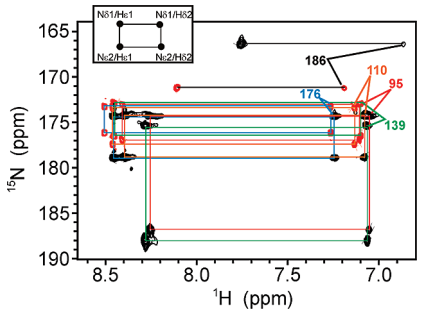

FIGURE 8: Long-range ^{1}H−^{15}N HMQC spectra of the histidine residues of wild-type PrP(89−230) at pH 5.5 (black) and pH 3.5 (red). Protonation states of histidines of wild-type mouse PrP(89−230) in pH 5.5 and 3.5 at 292 K are inferred from ^{15}Nδ1 and ^{15}Nε2 chemical shifts. The positions of the cross-peaks expected between the histidine ring nuclei when the ring is fully protonated are mapped in the top left corner. The ^{15}Nε2 resonance of H186 was not observed at either pH. Assignments of the five histidines are outlined in red (H95), orange (H110), green (H139), blue (H176), and black (H186).

protonated at pH 5.5; H95, H139, and H186 are partially deprotonated at pH 5.5 but become protonated at pH 3.5 (Supporting Information Table S2 and Figure 8), indicating that the pK_as of H95, H139, and H186 imidazole side chain are substantially lower than the typical pK_a value (6.6 ± 1); significantly lowered pK_a values are frequently observed for histidines located in the interior of proteins (*59*−*61*). Theoretical pK_a calculations also estimate a consistently low pK_a for H186 (*62*), supporting the notion that the low pK_a of H186 is due to its partially buried environment. In addition, the broad lines of the H186 imidazole resonances in the HMQC spectrum at both pH 5.5 and pH 3.5 (Figure 8) suggest the presence of chemical exchange on a microsecond to millisecond time scale.

It is surprising that H95 and H139 display pK_as as low as H186, despite their apparent surface exposure. There do not appear to be substantial chemical shift differences in the vicinity of these residues upon pH change, in contrast to H186 (Figure 3). The low pK_as of the H95 and H139 imidazoles may be due to dynamic effects such as transient hydrophobic or electrostatic interactions.

DISCUSSION

The initiation and subsequent process of the conformational changes in prion proteins that ultimately lead to onset of disease are not well understood. Our study with wild-type and four mutant PrPs at two pHs suggests that the segment spanning the C-terminal half of the α2 helix to the beginning of α3 (residues ≈187−197) may initiate conformational changes among inherited pathogenic, dominant negative mutants and wild-type PrP. Many of the pathogenic mutations causing GSS and familial CJD (H186R, T187R, T187K, T187A, E195K, and E199K; residue numbers as in mouse PrP) are clustered in this region (*63*). Notably, some individuals carrying the H186R mutation develop neurological dysfunction in childhood (*19*). At acidic pH, the positive charge introduced by protonation of the partially buried H186 disrupts the surrounding hydrophobic interactions, resulting in destabilization of the C-terminal half of α2. Low pH has been reported to trigger dramatically increased exposure of hydrophobic residues on the surface of PrP (*64*), and molecular dynamic simulations of human PrP suggest disruption of the C-terminal half of α2 under mildly acidic conditions (*65*). In addition, the amino acid sequence of helix α2 (DCVNITIKQHTVTTTTKG) includes many features that are atypical, including a sequence of β-branched side chains, TVTTTT (187−192), that is rare in the context of a helical conformation; such stretches are usually found in β-strand and loop conformations (*66*). Even though we identified a dynamically labile site by applying a pH change, the conformation and dynamics of this site may also be susceptible to changes induced by other factors such as hydrophobic and electrostatic perturbations.

In accord with our results, molecular dynamics simulations of the helices from mouse PrP showed that the C-terminal half of α2 (residues 184−194) and parts of α3 (residues 200−204 and 215−223) undergo transitions from α-helical structure to a β and/or random coil state (*66*). High-pressure NMR data also showed that a metastable conformer of PrP existing at ≈1% population has disordered α2 and α3 at pH 5.2 and 30 °C (*67*). Further support is provided by a recent *in silico* screening based on the differential dynamics of this region: a compound was discovered that specifically binds the region from α2 (V189, T192, and K194) to the α2−α3 loop (E196) and inhibits formation of PrP^{Sc} (*68*).

The amino acid sequence of the C-terminal half of α2 is well conserved among mammalian PrPs from different species (*69*) but is divergent for nonmammalian PrPs such as chickens, turtles, and frogs in which there are no reports of prion diseases (*70*). This region may therefore have a role in the cellular function of mammalian PrPs: deletion of the corresponding segment of the prion protein paralogue Doppel (Dpl) abolishes its neurotoxic effect (*71*). Dpl has ≈25% sequence identity with PrP and causes late-onset ataxia when overexpressed in the absence of cellular PrP (*72*). Dpl has the same topology as PrP but the C-terminal region of α2 is kinked at the residue that corresponds to T187 in mouse PrP (*73*); flexibility of this and following residues in Dpl closely matches our results for PrP (*73*).

Many of the inherited pathogenic mutations in the human PrP gene are located in residues 177−219, and the majority of them are associated with change of electrostatic charge (D178N, H187R, T188R, T188K, E196K, E200K, D202N, R208H, E211Q, Q217R, and E219K; residue numbers as in human PrP) (*1*−*4*). Since the proteins corresponding to many inherited disease-causing PrP mutations are as stable as wild-type PrP (*74*, *75*), the effect of the pathogenic PrP mutation is unlikely to be related to the thermodynamics of PrP in the native state. In addition, the solution structure of a pathogenic human PrP mutant (E200K) is nearly identical to that of the wild type (*76*). In line with these observations, comparison of the chemical shift differences and backbone dynamics of wild type and P101L, Q167R, H186R, and Q218K mutants of the mouse PrPs in this study shows that none of these mutations leads to major conformational and dynamical changes relative to the wild type. An exception is the H186R mutant PrP that displays inherent, pH-independent flexibility at the C-terminal half of α2, demonstrating the importance of the H186 protonation state and the consequent disruption of nearby hydrophobic interactions for the destabilization of PrP structure at this site. Our data raise the possibility that the pathogenic or dominant negative mutations exert their effects on some non-native intermediate form such as PrP* after conversion of PrP^{C} into PrP^{Sc} has been initiated. Depending on the amino acid substitution, rearrangements of hydrophobic groups can be facilitated or inhibited depending on the nature of the charge disturbance.

ACKNOWLEDGMENT

We thank John Chung and Gerard Kroon for assistance with NMR experiments and Professor Gerald Stubbs for helpful suggestions and a critical reading of the manuscript.

SUPPORTING INFORMATION AVAILABLE

The ^{15}N relaxation rates and analysis, the backbone assignments of the H186R, and the side chain assignments of histidines. This material is available free of charge via the Internet at http://pubs.acs.org.

REFERENCES

1. Prusiner, S. B. (1998) Prions. *Proc. Natl. Acad. Sci. U.S.A. 95*, 13363–13383.
2. Weissmann, C. (2004) The state of the prion. *Nat. Rev. Microbiol. 2*, 861–871.
3. Caughey, B., and Baron, G. S. (2006) Prions and their partners in crime. *Nature 443*, 803–810.
4. Aguzzi, A., Sigurdson, C., and Heikenwaelder, M. (2008) Molecular mechanisms of prion pathogenesis. *Annu. Rev. Pathol. 3*, 11–40.
5. Riek, R., Hornemann, S., Wider, G., Billeter, M., Glockshuber, R., and Wüthrich, K. (1996) NMR structure of the mouse prion protein domain PrP(121−231). *Nature 382*, 180–182.
6. Donne, D. G., Viles, J. H., Groth, D., Mehlhorn, I., James, T. L., Cohen, F. E., Prusiner, S. B., Wright, P. E., and Dyson, H. J. (1997) Structure of the recombinant full-length hamster prion protein PrP-(29−231): The N terminus is highly flexible. *Proc. Natl. Acad. Sci. U.S.A. 94*, 13452–13457.
7. Caughey, B. W., Dong, A., Bhat, K. S., Ernst, D., Hayes, S. F., and Caughey, W. S. (1991) Secondary structure analysis of the scrapie-associated protein PrP 27−30 in water by infrared spectroscopy. *Biochemistry 30*, 7672–7680.
8. Pan, K.-M., Baldwin, M., Nguyen, J., Gasset, M., Serban, A., Groth, D., Mehlhorn, I., Huang, Z., Fletterick, R. J., Cohen, F. E., and Prusiner, S. B. (1993) Conversion of α-helices into β-sheets features in the formation of the scrapie prion proteins. *Proc. Natl. Acad. Sci. U.S.A. 90*, 10962–10966.
9. Safar, J. G., Geschwind, M. D., Deering, C., Didorenko, S., Sattavat, M., Sanchez, H., Serban, A., Vey, M., Baron, H., Giles, K., Miller, B. L., DeArmond, S. J., and Prusiner, S. B. (2005) Diagnosis of human prion disease. *Proc. Natl. Acad. Sci. U.S.A. 102*, 3501–3506.
10. Caughey, B., Race, R. E., Ernst, D., Buchmeier, M. J., and Chesebro, B. (1989) Prion protein biosynthesis in scrapie-infected and uninfected neuroblastoma cells. *J. Virol. 63*, 175–181.
11. Borchelt, D. R., Scott, M., Taraboulos, A., Stahl, N., and Prusiner, S. B. (1990) Scrapie and cellular prion proteins differ in their kinetics of synthesis and topology in cultured cells. *J. Cell Biol. 110*, 743–752.
12. Caughey, B., and Raymond, G. J. (1991) The scrapie-associated form of PrP is made from a cell surface precursor that is both protease- and phospholipase-sensitive. *J. Biol. Chem. 266*, 18217–18223.
13. Borchelt, D. R., Taraboulos, A., and Prusiner, S. B. (1992) Evidence for synthesis of scrapie prion proteins in the endocytic pathway. *J. Biol. Chem. 267*, 16188–16199.
14. Zou, W. Q., and Cashman, N. R. (2002) Acidic pH and detergents enhance in vitro conversion of human brain PrP^{C} to a PrP^{Sc}-like form. *J. Biol. Chem. 277*, 43942–43947.
15. Hornemann, S., and Glockshuber, R. (1998) A scrapie-like unfolding intermediate of the prion protein domain PrP(121−231) induced by acidic pH. *Proc. Natl. Acad. Sci. U.S.A. 95*, 6010–6014.
16. Riek, R., Wider, G., Billeter, M., Hornemann, S., Glockshuber, R., and Wüthrich, K. (1998) Prion protein NMR structure and familial human spongiform encephalopathies. *Proc. Natl. Acad. Sci. U.S.A. 95*, 11667–11672.
17. Hart, T., Hosszu, L. L. P., Trevitt, C. R., Jackson, G. S., Waltho, J. P., Collinge, J., and Clarke, A. R. (2009) Folding kinetics of the human prion protein probed by temperature jump. *Proc. Natl. Acad. Sci. U.S.A. 106*, 5651–5656.
18. Hsiao, K., Baker, H. F., Crow, T. J., Poulter, M., Owen, F., Terwilliger, J. D., Westaway, D., Ott, J., and Prusiner, S. B. (1989) Linkage of a prion protein missense variant to Gerstmann-Sträussler syndrome. *Nature 338*, 342–345.
19. Hall, D. A., Leehey, M. A., Filley, C. M., Steinbart, E., Montine, T., Schellenberg, G. D., Bosque, P., Nixon, R., and Bird, T. (2005) PRNP H187R mutation associated with neuropsychiatric disorders in childhood and dementia. *Neurology 64*, 1304–1306.
20. Westaway, D., Zuliani, V., Cooper, C. M., Da Costa, M., Neuman, S., Jenny, A. L., Detwiler, L., and Prusiner, S. B. (1994) Homozygosity for prion protein alleles encoding glutamine-171 renders sheep susceptible to natural scrapie. *Genes Dev. 8*, 959–969.
21. Shibuya, S., Higuchi, J., Shin, R. W., Tateishi, J., and Kitamoto, T. (1998) Codon 219 Lys allele of PRNP is not found in sporadic Creutzfeldt-Jakob disease. *Ann. Neurol. 43*, 826–828.
22. Perrier, V., Kaneko, K., Safar, J., Vergara, J., Tremblay, P., DeArmond, S. J., Cohen, F. E., Prusiner, S. B., and Wallace, A. C. (2002) Dominant-negative inhibition of prion replication in transgenic mice. *Proc. Natl. Acad. Sci. U.S.A. 99*, 13079–13084.
23. Mehlhorn, I., Groth, D., Stockel, J., Moffat, B., Reilly, D., Yansura, D., Willett, W. S., Baldwin, M., Fletterick, R., Cohen, F. E., Vandlen, R., Henner, D., and Prusiner, S. B. (1996) High-level expression and characterization of a purified 142-residue polypeptide of the prion protein. *Biochemistry 35*, 5528–5537.
24. Clore, G. M., and Gronenborn, A. M. (1994) Multidimensional heteronuclear nuclear magnetic resonance of proteins. *Methods Enzymol. 239*, 349–363.
25. Liu, H., Farr-Jones, S., Ulyanov, N. B., Llinas, M., Marqusee, S., Groth, D., Cohen, F. E., Prusiner, S. B., and James, T. L. (1999) Solution structure of Syrian hamster prion protein rPrP(90−231). *Biochemistry 38*, 5362–5377.
26. Gossert, A. D., Bonjour, S., Lysek, D. A., Fiorito, F., and Wüthrich, K. (2005) Prion protein NMR structures of elk and of mouse/elk hybrids. *Proc. Natl. Acad. Sci. U.S.A. 102*, 646–650.
27. Yamazaki, T., Forman-Kay, J. D., and Kay, L. E. (1993) Two-dimensional NMR experiments for correlating $^{13}C\beta$ and $^{1}H\delta/\varepsilon$ chemical shifts of aromatic residues in ^{13}C-labeled proteins via scalar couplings. *J. Am. Chem. Soc. 115*, 11054–11055.
28. Bax, A., Ikura, M., Kay, L. E., Torchia, D. A., and Tschudin, R. (1990) Comparison of different modes of two-dimensional reverse-correlation NMR for the study of proteins. *J. Magn. Reson. 86*, 304–318.
29. Pelton, J. G., Torchia, D. A., Meadow, N. D., and Roseman, S. (1993) Tautomeric states of the active-site histidines of phosphorylated and unphosphorylated III^{Glc}, a signal-transducing protein from *Escherichia coli*, using two-dimensional heteronuclear NMR techniques. *Protein Sci. 2*, 543–558.
30. Farrow, N. A., Muhandiram, R., Singer, A. U., Pascal, S. M., Kay, C. M., Gish, G., Shoelson, S. E., Pawson, T., Forman-Kay, J. D., and Kay, L. E. (1994) Backbone dynamics of a free and a phosphopeptide-complexed Src homology 2 domain studied by ^{15}N NMR relaxation. *Biochemistry 33*, 5984–6003.
31. Farrow, N. A., Zhang, O., Forman-Kay, J. D., and Kay, L. E. (1995) Comparison of the backbone dynamics of a folded and an unfolded SH3 domain existing in solution in aqueous buffer. *Biochemistry 34*, 868–878.
32. Delaglio, F., Grzesiek, S., Vuister, G. W., Guang, Z., Pfeifer, J., and Bax, A. (1995) NMRPipe: a multidimensional spectral processing system based on UNIX pipes. *J. Biomol. NMR 6*, 277–293.
33. Farrow, N. A., Zhang, O., Forman-Kay, J. D., and Kay, L. E. (1994) A heteronuclear correlation experiment for simultaneous determination of ^{15}N longitudinal decay and chemical exchange rates of systems in slow equilibrium. *J. Biomol. NMR 4*, 727–734.
34. Tjandra, N., Szabo, A., and Bax, A. (1996) Protein backbone dynamics and ^{15}N chemical shift anisotropy from quantitative measurement of relaxation interference effects. *J. Am. Chem. Soc. 118*, 6986–6991.
35. Lipari, G., and Szabo, A. (1982) Model-free approach to the interpretation of nuclear magnetic resonance relaxation in macromolecules. 2. Analysis of experimental results. *J. Am. Chem. Soc. 104*, 4559–4570.
36. Lipari, G., and Szabo, A. (1982) Model-free approach to the interpretation of nuclear magnetic resonance relaxation in macromolecules. 1. Theory and range of validity. *J. Am. Chem. Soc. 104*, 4546–4559.
37. Clore, G. M., Szabo, A., Bax, A., Kay, L. E., Driscoll, P. C., and Gronenborn, A. M. (1990) Deviations from the simple two-parameter model-free approach to the interpretation of nitrogen-15 nuclear magnetic relaxation of proteins. *J. Am. Chem. Soc. 112*, 4989–4991.
38. Bae, S. H., Dyson, H. J., and Wright, P. E. (2009) Prediction of the rotational tumbling time for proteins with disordered segments. *J. Am. Chem. Soc. 131*, 6814–6821.
39. d'Auvergne, E. J., and Gooley, P. R. (2003) The use of model selection in the model-free analysis of protein dynamics. *J Biomol. NMR 25*, 25–39.

40. d'Auvergne, E. J., and Gooley, P. R. (2006) Model-free model elimination: a new step in the model-free dynamic analysis of NMR relaxation data. *J. Biomol. NMR 35*, 117–135.
41. Farrow, N. A., Zhang, O., Szabo, A., Torchia, D. A., and Kay, L. E. (1995) Spectral density function mapping using ^{15}N relaxation data exclusively. *J. Biomol. NMR 6*, 153–162.
42. Palmer, A. G., Kroenke, C. D., and Loria, J. P. (2001) Nuclear magnetic resonance methods for quantifying microsecond-to-millisecond motions in biological macromolecules. *Methods Enzymol. 339*, 204–238.
43. Altieri, A. S., Hinton, D. P., and Byrd, R. A. (1995) Association of biomolecular systems via pulsed field gradient NMR self-diffusion measurements. *J. Am. Chem. Soc. 117*, 7566–7567.
44. Calzolai, L., and Zahn, R. (2003) Influence of pH on NMR structure and stability of the human prion protein globular domain. *J. Biol. Chem. 278*, 35592–35596.
45. Gerber, R., Tahiri-Alaoui, A., Hore, P. J., and James, W. (2007) Oligomerization of the human prion protein proceeds via a molten globule intermediate. *J. Biol. Chem. 282*, 6300–6307.
46. Halle, B., and Davidovic, M. (2003) Biomolecular hydration: From water dynamics to hydrodynamics. *Proc. Natl. Acad. Sci. U.S.A. 100*, 12135–12140.
47. Viles, J. H., Donne, D. G., Kroon, G. J. A., Prusiner, S. B., Cohen, F. E., Dyson, H. J., and Wright, P. E. (2001) Local structural plasticity of the prion protein. Analysis of NMR relaxation dynamics. *Biochemistry 40*, 2743–2753.
48. Ebert, M. O., Bae, S. H., Dyson, H. J., and Wright, P. E. (2008) NMR relaxation study of the complex formed between CBP and the activation domain of the nuclear hormone receptor coactivator ACTR. *Biochemistry 47*, 1299–1308.
49. O'Sullivan, D. B., Jones, C. E., Abdelraheim, S. R., Brazier, M. W., Toms, H., Brown, D. R., and Viles, J. H. (2009) Dynamics of a truncated prion protein, PrP(113-231), from ^{15}N NMR relaxation: order parameters calculated and slow conformational fluctuations localized to a distinct region. *Protein Sci. 18*, 410–423.
50. Chen, J., Brooks, C. L., and Wright, P. E. (2004) Model-free analysis of protein dynamics: assessment of accuracy and model selection protocols based on molecular dynamics simulations. *J. Biomol. NMR 29*, 243–257.
51. Schurr, J. M., Babcock, H. P., and Fujimoto, B. S. (1994) A test of the model-free formulas. Effects of anisotropic rotational diffusion and dimerization. *J. Magn. Reson. B 105*, 211–224.
52. Kroenke, C. D., Loria, J. P., Lee, L. P., Rance, M., and Palmer, A. G. (1998) Longitudinal and transverse ^{1}H-^{15}N dipolar/^{15}N chemical shift anisotropy relaxation interference: unambiguous determination of rotational diffusion tensors and chemical exchange effects in biological macromolecules. *J. Am. Chem. Soc. 120*, 7905–7915.
53. Sigurdson, C. J., and Aguzzi, A. (2007) Chronic wasting disease. *Biochim. Biophys. Acta 1772*, 610–618.
54. Christen, B., Perez, D. R., Hornemann, S., and Wüthrich, K. (2008) NMR structure of the bank vole prion protein at 20 degrees C contains a structured loop of residues 165−171. *J. Mol. Biol. 383*, 306–312.
55. Sigurdson, C. J., Nilsson, K. P., Hornemann, S., Heikenwalder, M., Manco, G., Schwarz, P., Ott, D., Rulicke, T., Liberski, P. P., Julius, C., Falsig, J., Stitz, L., Wüthrich, K., and Aguzzi, A. (2009) De novo generation of a transmissible spongiform encephalopathy by mouse transgenesis. *Proc. Natl. Acad. Sci. U.S.A. 106*, 304–309.
56. Lysek, D. A., Schorn, C., Nivon, L. G., Esteve-Moya, V., Christen, B., Calzolai, L., Von Schroetter, C., Fiorito, F., Herrmann, T., Güntert, P., and Wüthrich, K. (2005) Prion protein NMR structures of cats, dogs, pigs, and sheep. *Proc. Natl. Acad. Sci. U.S.A. 102*, 640–645.
57. Lopez Garcia, F., Zahn, R., Riek, R., and Wüthrich, K. (2000) NMR structure of the bovine prion protein. *Proc. Natl. Acad. Sci. U.S.A. 97*, 8334–8339.
58. Zahn, R., Liu, A., Luhrs, T., Riek, R., Von Schroetter, C., Lopez, G. F., Billeter, M., Calzolai, L., Wider, G., and Wüthrich, K. (2000) NMR solution structure of the human prion protein. *Proc. Natl. Acad. Sci. U.S.A. 97*, 145–150.
59. Edgcomb, S. P., and Murphy, K. P. (2002) Variability in the pKa of histidine side-chains correlates with burial within proteins. *Proteins 49*, 1–6.
60. Plesniak, L. A., Connelly, G. P., Wakarchuk, W. W., and McIntosh, L. P. (1996) Characterization of a buried neutral histidine residue in *Bacillus circulans* xylanase: NMR assignments, pH titration, and hydrogen exchange. *Protein Sci. 5*, 2319–2328.
61. Yu, L., and Fesik, S. W. (1994) pH titration of the histidine residues of cyclophilin and FK506 binding protein in the absence and presence of immunosuppressant ligands. *Biochim. Biophys. Acta 1209*, 24–32.
62. Gordon, J. C., Myers, J. B., Folta, T., Shoja, V., Heath, L. S., and Onufriev, A. (2005) H++: a server for estimating pKas and adding missing hydrogens to macromolecules. *Nucleic Acids Res. 33*, W368–W371.
63. Kong, Q., Surewicz, W. K., Petersen, R. B., Zou, W., Chen, S. G., Gambetti, P., Parch, P., Capellari, S., Goldfarb, L., Montagna, P., Lugaresi, E., Piccardo, P., and Ghetti, B. (2004) Inherited prion diseases, in Prion Biology and Diseases (Prusiner, S. B., Ed.) 2nd ed., pp 673−775, Cold Spring Harbor Press, Cold Spring Harbor, NY.
64. Swietnicki, W., Petersen, R., Gambetti, P., and Surewicz, W. K. (1997) pH-dependent stability and conformation of the recombinant human prion protein PrP(90−231). *J. Biol. Chem. 272*, 27517–27520.
65. Langella, E., Improta, R., and Barone, V. (2004) Checking the pH-induced conformational transition of prion protein by molecular dynamics simulations: Effect of protonation of histidine residues. *Biophys. J. 87*, 3623–3632.
66. Dima, R. I., and Thirumalai, D. (2004) Probing the instabilities in the dynamics of helical fragments from mouse PrP^{C}. *Proc. Natl. Acad. Sci. U.S.A. 101*, 15335–15340.
67. Kuwata, K., Li, H., Yamada, H., Legname, G., Prusiner, S. B., Akasaka, K., and James, T. L. (2002) Locally disordered conformer of the hamster prion protein: a crucial intermediate to PrP^{Sc}? *Biochemistry 41*, 12277–12283.
68. Kuwata, K., Nishida, N., Matsumoto, T., Kamatari, Y. O., Hosokawa-Muto, J., Kodama, K., Nakamura, H. K., Kimura, K., Kawasaki, M., Takakura, Y., Shirabe, S., Takata, J., Kataoka, Y., and Katamine, S. (2007) Hot spots in prion protein for pathogenic conversion. *Proc. Natl. Acad. Sci. U.S.A. 104*, 11921–11926.
69. Billeter, M., Riek, R., Wider, G., Hornemann, S., Glockshuber, R., and Wüthrich, K. (1997) Prion protein NMR structure and species barrier for prion diseases. *Proc. Natl. Acad. Sci. U.S.A. 94*, 7281–7285.
70. Calzolai, L., Lysek, D. A., Perez, D. R., Güntert, P., and Wüthrich, K. (2005) Prion protein NMR structures of chickens, turtles, and frogs. *Proc. Natl. Acad. Sci. U.S.A. 102*, 651–655.
71. Drisaldi, B., Coomaraswamy, J., Mastrangelo, P., Strome, B., Yang, J., Watts, J. C., Chishti, M. A., Marvi, M., Windl, O., Ahrens, R., Major, F., Sy, M. S., Kretzschmar, H., Fraser, P. E., Mount, H. T., and Westaway, D. (2004) Genetic mapping of activity determinants within cellular prion proteins: N-terminal modules in PrP^{C} offset pro-apoptotic activity of the Doppel helix B/B′ region. *J. Biol. Chem. 279*, 55443–55454.
72. Qin, K., O'Donnell, M., and Zhao, R. Y. (2006) Doppel: more rival than double to prion. *Neuroscience 141*, 1–8.
73. Mo, H., Moore, R. C., Cohen, F. E., Westaway, D., Prusiner, S. B., Wright, P. E., and Dyson, H. J. (2001) Two different neurodegenerative diseases caused by proteins with similar structures. *Proc. Natl. Acad. Sci. U.S.A. 98*, 2352–2357.
74. Liemann, S., and Glockshuber, R. (1999) Influence of amino acid substitutions related to inherited human prion diseases on the thermodynamic stability of the cellular prion protein. *Biochemistry 38*, 3258–3267.
75. Swietnicki, W., Petersen, R. B., Gambetti, P., and Surewicz, W. K. (1998) Familial mutations and the thermodynamic stability of the recombinant human prion protein. *J. Biol. Chem. 273*, 31048–31052.
76. Zhang, Y. B., Swietnicki, W., Zagorski, M. G., Surewicz, W. K., and Sönnichsen, F. D. (2000) Solution structure of the E200K variant of human prion protein - Implications for the mechanism of pathogenesis in familial prion diseases. *J. Biol. Chem. 275*, 33650–33654.